Proceedings of the INMM & ESARDA Joint Virtual Annual Meeting
August 23-26 & August 30-September 1, 2021

DEVELOPMENT OF A POWDER BED ELECTRON BEAM ADDITIVE MANUFACTURING (EBAM) PARAMETER SET FOR PRINTING FULLY DENSE, CRACK-FREE, MOLYBDENUM PARTS

Andrew H. Chern[a] (ahchern@bwxt.com) **Daniel W. Galicki**[a*] (dwgalicki@bwxt.com) **Travis A. McFalls**[a] (tamcfalls@bwxt.com) **Travis B. Fritts**[a] (tbfritts@bwxt.com) **Ryan S. Kitchen**[a] (rskitchen@bwxt.com)

[a]BWX Technologies, Inc. (BWXT), Lynchburg, VA; *Corresponding author

ABSTRACT

This study reports the methods used by BWX Technologies' additive manufacturing (AM) division to obtain electron beam additive manufacturing (EBAM) parameter sets that enable the printing of crack-free, fully dense, pure molybdenum AM parts. Special focus is also given to explaining the unique capabilities of the machine used during the study; an Arcam Spectra H.

1. INTRODUCTION/BACKGROUND

1.1 Pure Molybdenum as a candidate for EBM AM

Molybdenum is a refractory metal with a melting temperature of 2623°C and excellent material properties at high temperatures. It is also creep resistant at high temperatures and has one of the lowest coefficients of thermal expansion of any metal. These features make molybdenum a strong candidate for any kind of structural applications at very high temperatures such as those that exist in very high temperature gas reactor (VHTGR) designs or in designs for nuclear powered rockets for transit in space. Specific to its applicability as a nuclear reactor component, many of the existing molybdenum alloys, such as those containing rhenium to increase the ductility of the alloy, are neutronically disadvantageous. Pure molybdenum has favorable neutronic properties but is difficult to manufacture and shape due to its high ductile to brittle temperature and its tendency to oxidize in atmosphere. It is these features that make pure molybdenum an excellent candidate for processing via electron beam additive manufacturing (AM). Electron beam AM operates in a vacuum and at very high temperatures, avoiding molybdenum's ductile to brittle temperature zone while simultaneously annealing out any internal stress developed during processing.

1.2 Challenges with Welding Pure Molybdenum

It is reasonable to regard powder bed additive manufacturing (AM) processes as consisting of a series of stacked welds, with the microstructure of the resulting additively manufactured part dependent on the complex thermal history that results from the repeated welding passes. It is therefore appropriate to provide a review of the welding literature for molybdenum in order to gain some insight into how molybdenum might behave during an AM process and what kinds of mechanical properties one can expect from an additively manufactured molybdenum part. Much of the existing literature investigating the weldability of pure molybdenum (Mo) focuses on electron beam and gas-arc welding methods [1-4]. Traditionally, the four major issues that hinder the weldability of pure Mo are: 1) molybdenum's high ductile-to-brittle transition temperature (DBTT), 2) the formation of porosity within the weldment, 3) hot-cracking of the weldment during cool down and 4) abnormal grain growth [1].

Molybdenum, like many other body-centered cubic metals, is brittle at lower temperatures. However, the temperature at which pure molybdenum transitions from ductile to brittle deformation is higher than more common metals, like iron. This higher DBTT plays a significant role in the weldability of pure Mo. Contaminates such as oxygen and nitrogen have been shown to reduce ductility and increase the DBTT, with O having the greatest effect per weight percent added [2]. Oxides and nitrides have also been shown to segregate to grain boundaries within molybdenum, further decreasing the metal's ductility [3]. During

solidification and cool-down, it has been shown that oxide formation at grain boundaries can serve as initiation sites for cracks [1]. It is generally recommended to clean weldments chemically before welding to remove any oxide films that are present [2]. Morito has demonstrated that the addition of carbon and the precipitation of carbides within molybdenum can increase the ductility of the alloy by virtue of increased cohesion of grain boundaries [4].

In addition to the effects of chemical impurities in pure molybdenum, the welding method chosen can greatly affect the grain size, grain growth in weldments and the thickness of the heat-affected zone (HAZ), all of which can affect the mechanical behavior of the weldment. Electron beam welding (EBW) is generally preferable over arc-gas welding because the vacuum environment minimizes the formation of oxides and nitrides during welding and the high power density provided by the electron beam minimizes the resulting heat-affected zone. The high thermal gradients produced during EBW produce a more cellular microstructure in the weld which translates to a significant increase in hardness values over arc-gas welds [2-3].

1.3 Additive Manufacturing of Molybdenum

The majority of the limited data available in the open literature concerning additive manufacturing of pure molybdenum focuses on powder-bed selective laser melting [5-9] and electron beam direct energy deposition [10]. There is no open literature describing the additive manufacturing of molybdenum using the electron beam powder bed process. The existing literature results demonstrate that additive manufacturing of molybdenum faces similar issues as processing molybdenum by conventional methods like welding, but also problems unique to additive manufacturing; such as: oxygen contamination [8], cracking [5,6,8,10] and low density from insufficient energy input [7,9]. Researchers have attempted various mitigating techniques to address these problems with some success. Wang *et al.* make the claim to have successfully printed crack-free pure molybdenum using the laser powder bed fusion (L-PBF) process by building on top of support structures. The authors' reason for doing this was to thermally isolate the part by using the unmelted powder bed beneath the part as thermal insulation, allowing the part to retain heat and avoid stress-causing high thermal gradients during processing [5]. Kaserer *et al.* also observed cracking in L-PBF pure molybdenum, but found that alloying pure molybdenum with 0.45wt% carbon refined the grain structure and suppressed cracking by altering the solidification mode [6].

Applying suggested crack suppression methods learned from welding molybdenum, such as substrate preheating [11,12] and limiting oxygen exposure [11,13], have proven to be ineffective at suppressing cracks in L-PBF AM molybdenum, as cracks were still observed after printing on a heated build plate while also keeping build chamber O_2 content below 20 ppm [8]. Powder bed electron beam melting (EBM) has the capability to go beyond the limits of L-PBF processes and more effectively administer traditional welding crack-suppression methods. The vacuum environment and increased beam speed of EBM technology provides the opportunity to print traditionally crack-prone materials like pure molybdenum.

2. DESCRIPTION OF THE SPECTRA-H EBM MACHINE

The Arcam EBM Spectra H machine purchased by BWXT and used in this study was the first Spectra H in the U.S. sold to an entity outside of the Arcam's parent organization, GE. The Spectra H contains features specifically designed to enable the processing of high temperature materials that are lacking in previous Arcam EBM models. These features proved to be essential in additively manufacturing crack-free, dense molybdenum and are described in the following sections.

2.1 Special Features of the Arcam Spectra-H EBM Machine

The Spectra series is the newest release of Arcam GE's Electron Beam Additive machines. The Spectra H machine that was used in this study contains many new components that allow for improved processing of high-temperature, crack-prone materials over previous Arcam GE machine models.

2.1.1 Spectra-H Default Equipment

A moveable heat shield that raises to allow the rake to pass underneath and lowers during processing was added to the Spectra H. Allowing the heat shield to lower to near the powder bed surface during operation serves to contain radiative heat loss and limit heat loss from the powder bed during processing. Maintaining higher temperatures with less energy input is key to being able to produce dense, crack-free parts made of crack-prone materials, such as molybdenum. During operation, the heat shield raises to allow the rake system to distribute powder over the build area and lowers once raking is complete.

The raking system has also been overhauled in the Spectra H. Previous models used a powder sensor to determine the amount of powder distributed in every layer. The new system uses location set points for the rake to distribute the same amount of powder each and every time. New rake set points were calculated prior to beginning parameter development studies for molybdenum. The material specific set points allowed for powder distribution to remain constant during processing.

The Spectra H is capable of putting out 6kW of power using an increased max output electron beam current of 100mA. This allows the Spectra H to deposit the same amount of power as an earlier machine model would but in less time, decreasing the time between layer melting and allowing for increases in beam speed during melting. When processing crack-prone materials like molybdenum, this feature is especially helpful during the preheat stage when the electron beam is used to combat heat lost during the time it takes to melt by maintaining the powder bed at a desired processing temperature.

2.1.2 BWXT System Upgrades

Knowing the build plate temperature in real-time is a valuable tool when determining build plate heating parameters and can be a key indicator of build quality and build success. Monitoring the temperature of the powder bed also gives indication for when it is safe to remove a finished part from the Spectra H.

BWXT modified the default thermocouple system of the Spectra H used in this study to better capture the temperature of the build plate during processing. Standard Spectra H components include two thermocouples located beneath the leveling nuts that a build plate traditionally sits on. BWXT's proprietary processing method required specially designed thermocouples. BWXT routed a single K-type thermocouple up through the build platform to sit directly under, and touch, the underside of the build plate. The new thermocouple was plugged into the primary thermocouple port on the Spectra H which allowed monitoring of the build plate temperature using the Spectra H's human-machine interface (HMI).

2.2 Spectra-H In-Situ Monitoring and Imaging Equipment

Electron beam AM systems necessarily require more time between individual build cycles than L-PBF systems. This is driven by the system's need to pump down to vacuum and preheat the build plate prior to melting, as well as the cool down time required and the time it takes to re-pressurize the build chamber at the end of a build cycle. Therefore, each build in a parameter development cycle must be designed to maximize the amount of information obtained. The in-situ monitoring and data collection capabilities of the Spectra H were critical tools that increased the efficiency by which BWXT was able to develop build parameters to print crack-free pure molybdenum.

2.2.1 Spectra-H Default Equipment

The Spectra H includes a single, 26 megapixel monochrome camera equipped with a 30mm lens and a near infrared (NIR) pass filter, used for imaging the build plate and powder bed throughout the build. This camera is positioned outside the build chamber and behind a window with a mechanical shutter that protects the window from metallization due to vapor deposition during the build process. The camera's default field of view is windowed down to a 16 megapixel square, 1/3 of which contains the machine's build plate. This configuration offers a pixel size corresponding to approximately 90um x 90um of the build area.

A NIR image is captured after each layer is finished melting and after each rake operation in order to observe powder spreading. This imagery is used by operators to determine if the machine is operating properly and to identify geometric deviations and porosity in manufactured parts.

2.2.2 BWXT System Upgrades

BWXT outfitted the standard NIR camera on the Spectra H with a 50mm lens and modified the mounting angle to permit increased magnification of the build plate. Additionally, an external camera viewing system was connected to enable fine-tuned focus adjustments of the camera lens, providing much clearer imaging of the build plate. This configuration decreased the effective pixel size to 60um x 60um, providing finer details than the default lens. BWXT has also developed a proprietary software system that analyzes NIR images, automatically identifying porosity in printed parts and detecting and measuring printed geometries. The software is capable of collating the information gained from individual layer images into representative digital twins that can be further analyzed to provide information about porosity size, location and distribution within a printed part. Validation of the software's porosity detection capabilities was conducted by comparing against computed tomography (CT) scan data.

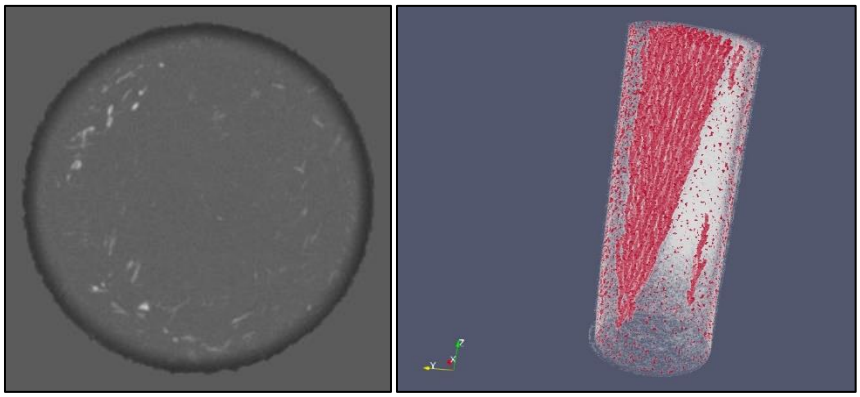

Figure 1: Near Infrared (NIR) image of the surface of a cylinder built using the Spectra H machine (a), Non-proprietary digital twin reconstruction of a cylinder built using the Spectra H and exhibiting columnar "chimney" porosity, identified by BWXT's proprietary porosity detection software system.

BWXT also modified the support structure of the Spectra H to permit the mounting of a FLIR 8501sc High Speed Infrared (HSIR) camera. HSIR imaging enables the real-time capture and imaging of thermal data during the extremely fast melt and cooling process, which permits later correlation to material and microstructural properties. The HSIR camera has a maximum resolution of 1280x1024 pixels at 180 frames per second (FPS). In this installation, it was configured to capture a smaller image size of 384x384 pixels at an increased framerate of 800 FPS. In some experimental cases, the image size was further decreased to 64x64 pixels to obtain a framerate of 3600 FPS with the goal of observing real time effects of high-speed beam rastering.

BWXT installed two extra monitors on the Spectra H above the standard human-machine interface monitor to enable real-time viewing of the HSIR camera output.

In order to capture imagery during the melt process, BWXT equipped the Spectra H with a custom-made viewing portal apparatus. This device consists of sapphire and leaded glass windows, which are protected from the weld process by means of a transparent Kapton film. This sacrificial film is placed in front of the glass window to prevent metal vapors from crystallizing on the surface of the glass, rendering the window opaque. An electric motor is used to periodically roll the film across the surface to replace it with new, clear film as it becomes metallized.

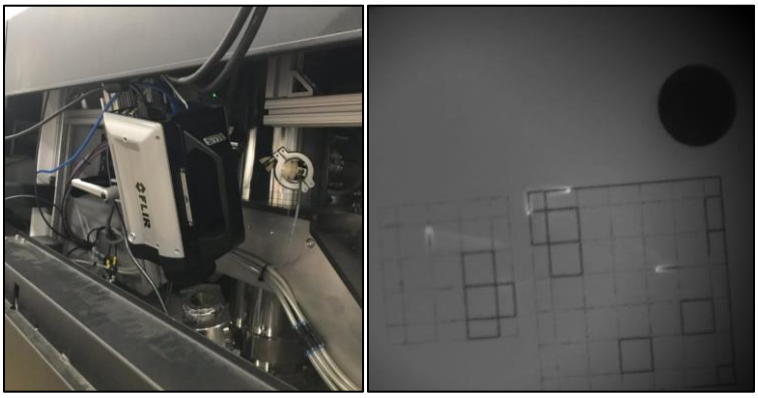

Figure 2: FLIR 8501sc High Speed Infrared (HSIR) camera mounted on Spectra H (a), Still-frame from a HSIR video recording multiple melt pools during the melting of support structure (b).

3. EXPERIMENT

The review of additive manufactured pure molybdenum literature revealed common problems across all studies; lack-of-fusion defects and low density from insufficient energy input, cracking, porosity and limited geometric build capabilities [5-10]. These four concerns were identified as the most significant barriers to successful and consistent prints. To address and solve these issues, an experimental design consisting of a 3x3 grid of 10 mm x 10 mm x 25 mm (length x width x height) rectangular blocks was developed. Figure 3 provides the position of each part on the build plate. Each block could be printed with its own Melt Theme. This design allowed for full parameter sweeps and the ability to obtain a parameter window in which successful builds could be obtained. Success criteria was determined by the presence of defects, flatness of top surface and adherence to geometric accuracy.

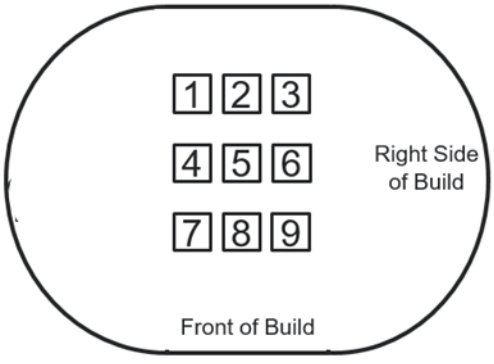

Figure 3: Schematic layout of 3x3 matrix of blocks arranged on the build plate.

Each build that was conducted as part of the parameter development effort was set up according to a BWXT-developed checklist to ensure build consistency. The checklist was posted in physical form on the door of the Spectra H and its adherence was confirmed by requiring operators to initial individual procedure steps as they were completed. In this way, variances between builds resulting from individual operator setup was considered reduced.

Two different virgin plasma-atomized molybdenum powder batches were purchased from Tekna and used as feedstock. Before use as feedstock, the powder was either stored in its factory-sealed containers or in the Spectra H powder hoppers under vacuum. Bulk chemistry of each powder batch was measured and results are provided in Table 1.

Table 1: Molybdenum powder feedstock chemistry results (wt%)

Powder Sample	Molybdenum	Tungsten	Oxygen	Carbon	Silicon	Iron	Nitrogen	Sulfur
Mo90-19008	99.97 ± 0.01	0.015 ± 0.002	0.010 ± 0.0005	0.003 ± 0.002	< 0.001 ± 0.001	< 0.0005 ± 0.0005	< 0.0005 ± 0.001	< 0.0005 ± 0.002
Mo90-19012	99.97 ± 0.01	0.015 ± 0.002	0.009 ± 0.0005	0.002 ± 0.002	< 0.001 ± 0.001	< 0.0005 ± 0.0005	< 0.0005 ± 0.001	< 0.0005 ± 0.002

Melt parameters most associated with energy density and energy input were selected as the independent variables. The parameters of interest included: Current Compensation [14], Focus Offset [15-17], Beam Current, Speed Function [16,18] and Turning Points Function [14,15,19]. The associated references contain descriptions of the parameters. Parameters not mentioned, including those in the Preheat Theme and Build Plate Heating Theme, are not listed for industrial confidentiality reasons. Over six separate builds, the parameters were adjusted and the results observed by optical microscopy, visual inspection of the part, analyses of NIR images and dimensional measurements.

It should be noted that for parts with Current Compensation set to TRUE, *RefCurrent* in the Current Compensation Function was set such that the calculated and output currents were equal to a specific current value across the longest scan length. In this experiment, the longest scan length was across the diagonal of any of the nine individual blocks, or 14.1421 mm.

4. RESULTS

4.1 Build 1

All nine parts in Build 1 used the same melt theme and defects were observed in the NIR images of all parts during the build. As shown in 4, the defects look like white speckles generally clustered in the center of each block. A block was sectioned along the long axis (to observe the Z plane) and in the transverse direction (to observe the XY plane), mounted and polished. Inspection of the polished surfaces revealed chimney-like defects extending multiple build layers (Figure 5). SEM images of a block's top surface (Figure 5 (c)) revealed partially-melted and un-melted powder particles inside the defects, indicating that the defects were caused by insufficient energy density and incomplete melting.

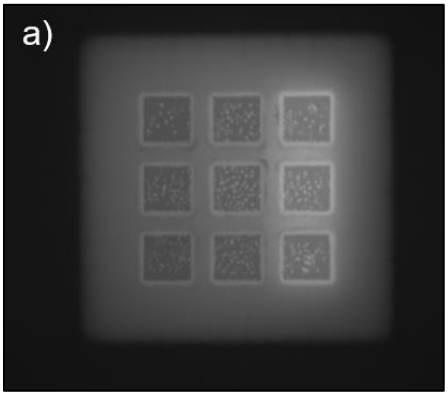

Figure 4: Example NIR image of Build 1 showing defects in all parts.

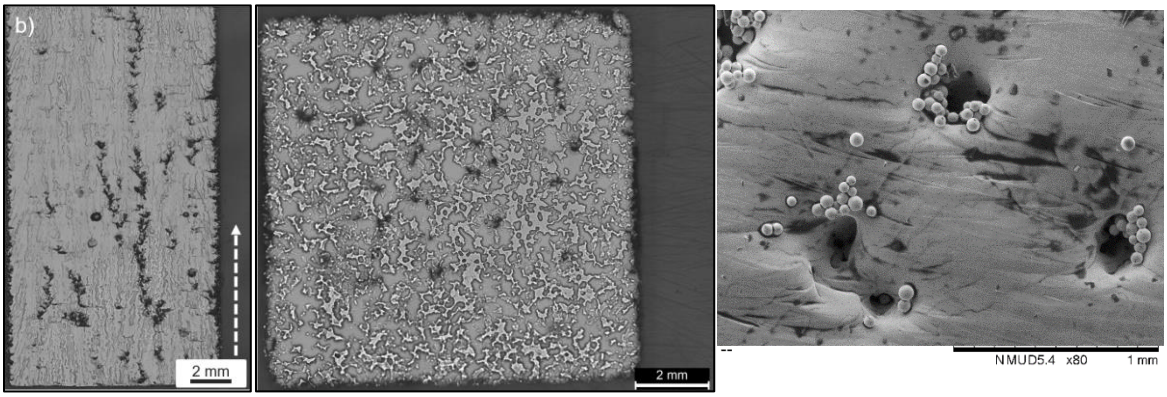

Figure 5: Sectioned and polished cross section of the Z plane (left) and of the XY plane (middle) revealing the chimney-type defects, white arrow indicates build direction. SEM image of the surface of a part with chimney-type interconnected porosity (right).

4.2 Build 2

Build 2 varied the Speed Function (SF) and hatch melt current. The NIR images captured during the build, along with optical microscopy inspection of sectioned parts along the long axis (to observe the Z plane) and in the transverse direction (to observe the XY plane), revealed that the parts melted with lowest Speed Function value contained the fewest defects. The most energy dense were melted with the highest current and lowest speed, Parts 4 and 7, showed the fewest defects and highest density.

Defects were observed in all blocks melted with higher Speed Function values as shown in Figure 6. An arc trip occurred after melting the layer at 15.5 mm of build height, which caused the machine the recover and then re-melt the same layer. After the arc trip event, defects did not form in the group that was melted using a moderately high Speed Function value and defects were less prevalent in the group of blocks melted using the highest Speed Function value.

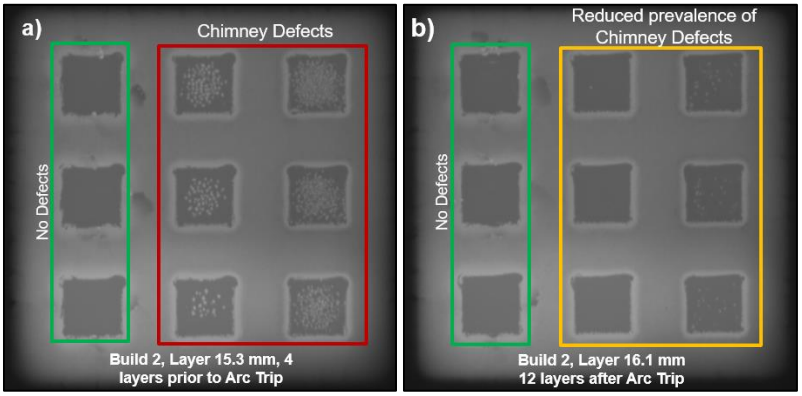

Figure 6: NIR Image of Build 2, four layers prior to an Arc Trip event (a) NIR image of Build 2, 12 layers after the Arc Trip event (b). The Arc Trip event caused the layer at 15.5 mm in build height to be melted twice.

4.3 Build 3

Blocks printed in Build 3 had the same melt themes as those printed in Build 2, but the Preheat Current and Repetitions parameter values were increased in an attempt to increase the powder bed surface temperature throughout the build. The NIR images revealed porosity in all parts except Part 7 (Figure 7) which was printed using the lowest Speed Function and highest melt current. It should be noted that the melt themes in Build 3 were identical to those in Build 2, with the only difference coming in the form of a higher temperature preheat. Even so, defects were observed in greater number in Build 3 than in Build 2. This indicates that the prevalence of the defects is not only dependent on Melt Themes, but also on other variables unknown at the time of printing.

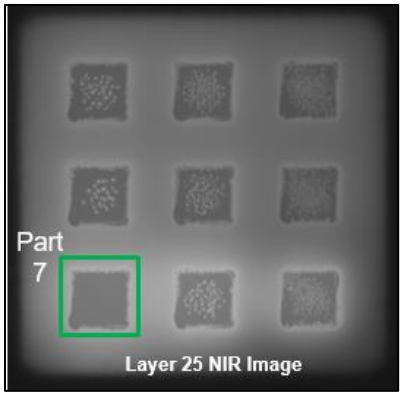

Figure 7: NIR image of Build 3, taken after the layer at 25 mm build height was melted, showing significant porosity in all parts except part 7.

4.4 Build 4

The goal of Build 4 was to alter the SF, melt current and Focus Offset values in an effort to increase beam speed while avoiding chimney porosity and achieving high density parts. The range of the Speed Function was reduced and the melt current range was increased.

NIR images revealed the absence of porosity in any of the blocks throughout the build, regardless of parameter set. Over-melting at the corners occurred because the Current Compensation function was not yet optimized.

As such, the beam current remained constant as the beam rastered diagonally; beginning at a corner, increasing in length at the diagonal widened, then decreasing in length as the diagonal shortened and finally finishing at the corner directly across from its starting point. The heat built up from melting the entire surface area of a block, as well as the fact that the beam current remains constant even while its raster area decreases, combine to result in an over-melt at the corner where the beam finishes rastering. A graphical representation of this phenomena is given in Figure 8.

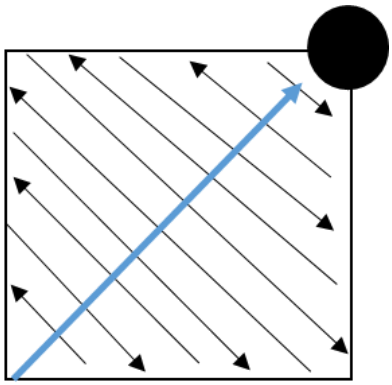

Figure 8: Schematic showing how heat accumulates during the melt raster scan with the Current Compensation function set to FALSE, resulting in over-melt at the corner of the part.

Part 5 was sectioned 5 mm from the top of the part in the transverse direction (to observe the XY plane). Figure 9 (b) is an optical micrograph of the polished cross-section. No cracking or defects were observed within the interior of the part, but several lack of fusion defects can be seen in the corners where over-melting occurred. The black dotted line in Figure 9 (b) is an artificial outline of the prescribed 10mm x 10mm cross-section geometry of the block as it was input into the Spectra H. It can be seen that the printed geometry does not match that of the design geometry, a problem closely associated with the Current Compensation function.

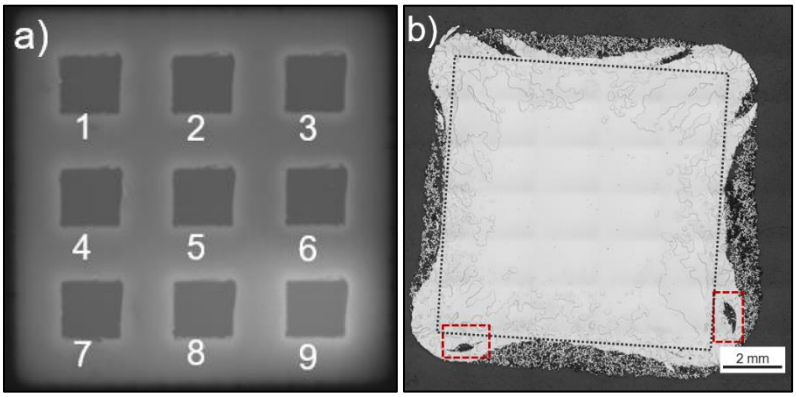

Figure 9: NIR Image of Build 4 revealing no porosity in Parts 1-9 (a) and a polished cross-section of Part 5 (b). The dotted black line in (b) outlines the 10 mm x 10 mm designed geometry and red dotted lines outline melt defects.

4.5 Build 5

The parts in Build 5 had the same Melt Themes as those in Build 4, but the Turning Points function was changed from FALSE to TRUE in an effort to improve geometric accuracy by reducing over-melt at the corners of the parts. The Turning Points function adjusts the speed of the beam near the edges of a part [14,15,19] and was not expected to have a significant influence on defects in the interior of the parts.

Build 5 failed at a build height of 9.5 mm because of smoking, but enough data was collected to make conclusions about the Melt Themes. Although the Melt Themes were identical to Build 4 with the exception of the Turning Points function, defects were observed in all parts except Part 7, as shown in the NIR image in Figure 10. The Turning Points function also did not seem to reduce the over-melting at the corners of the parts as expected. This result highlights the sensitivity of the AM process to seemingly minor parameter changes (i.e. toggling the Turning Points function).

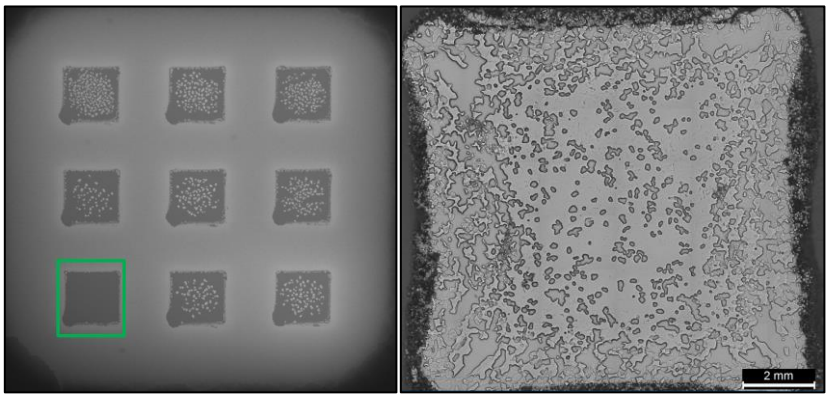

Figure 10: NIR image of Build 5, showing the over-melted corners in all 9 parts and defects in all parts except Part 7, which is outlined by the green box (left) Optical image of a Build 5 part sectioned in the XY plane and polished (right).

4.6 Build 6

In Build 6 the Melt Themes for Parts 1, 2, 3, 6 and 9 were duplicates of the Melt Themes for those Parts in Build 4. In an effort to reduce or eliminate the over-melting at the corners, the Melt Themes for Parts 4, 5, 7 and 8 varied the Speed Function, Focus, Turning Points and Current Compensation functions. The Current Compensation function parameters were set such that the melt current along the diagonal of the block was equal to the current used by the Melt Theme that produced the defect-free Part 7 in Build 5.

Inspection of the NIR images (Figure 11 (a)) for Build 6 revealed no porosity in any of the Parts, regardless of the Melt Themes. Although all of the Parts were considered defect-free, Part 4 had the flattest top surface by visual inspection and was the most geometrically accurate to the designed part (Figure 11 (b)). Judicious optimization of the Current Compensation (CC) and Turning Points (TP) Functions resulted in dense, geometrically accurate molybdenum parts.

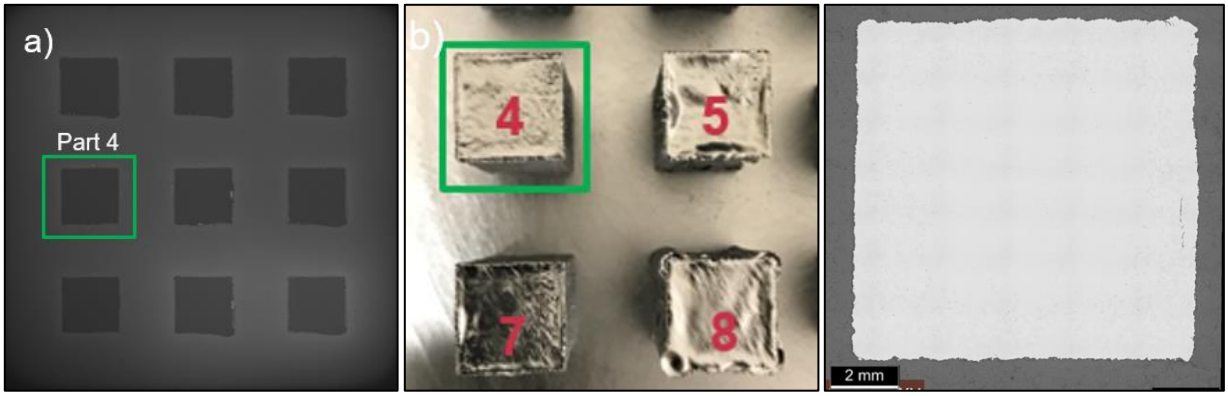

Figure 11: NIR Image of build 6 showing no porosity in any of the parts (a) and macrograph of the completed build highlighting Parts 4,5,7 and 8 (b). Optical image of Part 4 sectioned in the XY plane (c).

5. DISCUSSION

5.1 Chimney Defect Formation

The chimney-type pores that were observed in Builds 1, 2, 3 and 5 have been observed in other EBM builds using materials other than molybdenum [20-22]. However, the chimney defects observed in this EBM molybdenum study appear to nucleate in the interior of the part as opposed to at its edges. Chimney-type pores are created when the electron beam deposits insufficient energy to fully melt the powder bed and leaves un-melted powder particles in its wake. The un-melted particles are then buried beneath the next powder layer as it is deposited by the rake. Subsequent electron beam passes attempt to melt the freshly deposited powder but lacks the energy to re-melt the previous layer's powder below the recently deposited bed resulting in a pocket of partially melted powders. According to [22], the pore is filled and then the electron beam melts some of the top layer, creating a freely-suspended molten metal film which bursts and falls before it can solidify. The process repeats, layer after layer, resulting in a chimney defect filled with partially- or un-melted powder particles. Figure 12 provides a schematic showing how the chimney defects are created.

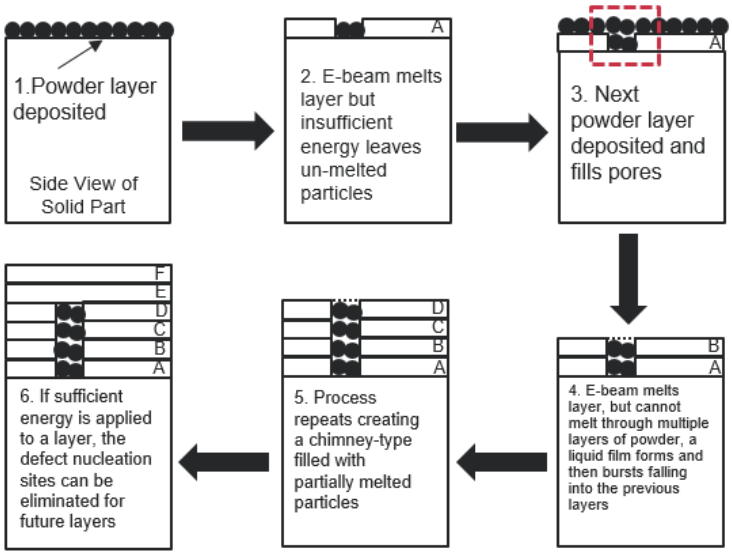

Figure 12: Schematic showing formation of chimney-type defects observed in the EBM molybdenum blocks.

In Build 5, the same defects were appearing in parts with high SF values. The higher beam speed resulted in lower local energy input and the creation of chimney-type pores. However, at layer 15.75 mm in Build 5, an arc trip occurred and the layer was melted twice, as usually happens after an arc-trip reset. After this arc trip, the defects began to disappear. The double-melt healed any lack-of-fusion defects and could penetrate into the chimney pores deep enough to create a fully consolidated layer, thus eliminating the pore nucleation sites as shown in step 6 of Figure 12.

5.2 Parameter Development

Over six successive builds, BWXT researchers developed a Melt Theme parameter set that produced fully-dense, crack-free and largely defect-free molybdenum parts. Sporadic lack-of-fusion defects and gas pores were occasionally observed, as is common in EBM components. The chimney-type defects extending multiple millimeters were not observed in parts build using the resulting Melt Theme, nor were any large areas of lack-of-fusion defects that are common in L-PBF molybdenum parts. Importantly, neither inter-granular solidification cracks, or cracks of any kind, were observed in the EBM molybdenum parts that were sectioned and imaged.

The parameter sets used in this study are plotted in Figure 13 and serve as a graphical representation of the processing parameter window that was developed during this study. Figure 13 does not contain parameter sets from Build 5, but does incorporate all of the parameter sets from Build 6. Marker size indicates the number of builds in which the parameter set was applied to a part. Green markers represent parameter sets that produced dense parts with no detected defects every time they were used, yellow markers indicate parameter sets that mostly produced dense parts but in one build produced a part with defects, orange markers represent parameter sets that built defect-free parts 50% of the time and red markers represent parameter sets that build parts containing many detected defects every time they were used.

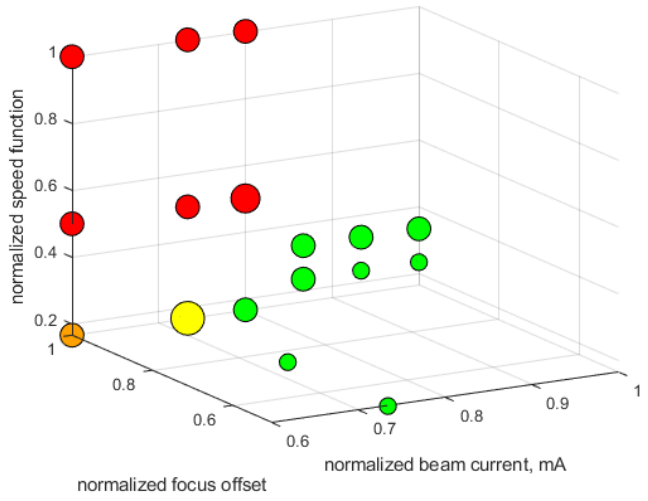

Figure 13: 3D scatter plot of normalized focus offset, beam current and speed function parameter sets used in this study. Marker color indicates success of a parameter set producing dense, defect-free parts (green=defect-free, red=lots of defects). Marker size indicates the number of builds where the parameter set was used.

The most optimized Melt Theme was that of Part 4 of Build 6. In comparison, the over-melted regions in the corners are observed in Part 8 of the same build. Part 8 was built with the same parameters as 4, with the exception of having CC and TP disabled. The CC function works by linearly increasing or reducing the melt

current depending on a geometric scan length in relation to a reference scan length. By utilizing this function in Part 4, the beam current was reduced as the beam approached the corners, thus eliminating the over-melted regions. The TP function was also enabled in Part 4 but, as Build 5 showed, it is likely that the CC function has a greater influence in controlling the geometric accuracy of a part than the TP function. The TP function works by controlling the speed of the beam as it scans closer to, or farther from, an edge of a part.

The Preheat parameters were also changed over the six builds and are summarized in Figure 14. The red and green outlined boxes indicate if the chimney-type defects were observed in the NIR images of builds.

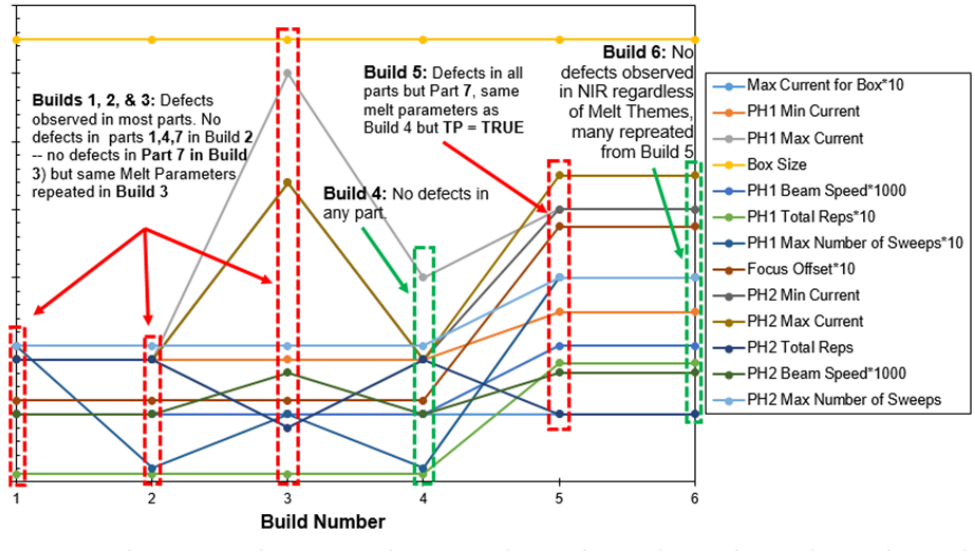

Figure 14: Graphical representation of Preheat parameters used by all six of the builds in this study.

Defects were observed in most of the parts printed in Builds 1, 2, & 3. Builds 2-3 were built using the exact same Melt Themes, but Build 3 utilized increased Preheat parameters. Parts 1, 4, & 7 in Build 2 contained very few defects throughout, while only Part 7 in Build 3 was defect-free. Build 4 contained no chimney defects in any of its Parts while utilizing the same preheat parameters as Builds 1 and 2, but different Melt Themes (mostly with lower Speed Function values). The Preheat was increased for Build 5 while maintaining the same Melt Themes that were used in Build 4, except for the activation of the Turning Points function. Similar to Build 3, increasing the Preheat parameters for Build 5 led to the formation of chimney defects throughout the build. Build 6 utilized the same Preheat as Build 5 and all parts in Build 6 were defect-free, but many of the same Melt Themes were utilized and the preheat was the same as Build 5.

The EBM process induces complicated heating cycles in both the parts being built and the powder bed surrounding the parts. All components within the build chamber are coupled from a heat transfer viewpoint, making it a challenging prospect to try to predict the behavior of the system in response to the heating cycles: Variations in energy input while building one part may influence an adjacent part in the same build, even if the two parts are printed with separate Themes. Even if processing parameters are kept constant from build to build, batch to batch powder feedstock variations (flow characteristics, packing density, etc.) may influence a build's thermal history. Human influence during build setup (minimized in this case through use of a standard setup procedure) has the potential to introduce unexpected variables into the execution of a build. An uncontrolled variable in this work that may also influence a build is the Grid Voltage value at the start of each build. The electron beam Grid Voltage is an electrical field in the Spectra H grid cup which controls the beam current. The higher the applied Grid Voltage, the lower the output current (1700V corresponds to a 0 mA

current) [23]. A low Grid Voltage value indicates that not enough electrons are being emitted from the cathode. The Grid Voltage and cathode are calibrated by the Spectra H machine using a black-box method prior to each build. When building with non-molybdenum materials, the authors have observed a pattern where a build will fail or contained significant part defects if the Grid Voltage was below 600V at the start of the build. The Grid Voltages of the builds in this study were not monitored.

6. CONCLUSIONS

Through a targeted parameter development campaign, BWXT's additive manufacturing division has developed an electron beam additive manufacturing parameter set that enables the production of crack-free, fully dense, geometrically accurate, pure molybdenum parts. The discovery of the parameter set was made possible by the enhanced capabilities of the Arcam Spectra H EBM machine in combination with proprietary in-situ monitoring and analysis software for detecting porosity in the AM parts. The installation of a high-speed infrared camera onto the Spectra H enabled real-time observation of the melt cycle which, in-turn, allowed the authors to make informed parameter changes during a build and receive immediate feedback from the machine.

ACKNOWLEDGMENTS

The authors would like to acknowledge their partnership with Oak Ridge National Laboratory (ORNL) that helped make this work possible. Personnel at ORNL's Manufacturing Demonstration Facility (MDF) provided valuable expert consultation, discussion and sample preparation services.

This material is based upon work supported by the Department of Energy under Award Number DE-NE0008744.

DISCLAIMER

REFERENCES

1) A.J. Moorehead, G.M. Slaughter, Welding studies of arc-cast molybdenum, *Welding Journal, 53(5) (1974), 185-191.*
2) N.E. Weare, R.E. Monroe, Welding and Brazing of Molybdenum, United States, 1959.
3) M. Kolarikova, L. Kolarik, P. Vondrous, Welding of Thin Molybdenum sheets by EBW and GTAW, *Proceedings of the 23rd International DAAAM Symposium, 23(1) (2012), 1005-1008.*
4) F. Morito, Effects of Impurities on the weldability of powder metallurgy, electron beam melted, and arc- melted molybdenum and its alloys, *Journal of Materials Science, 24 (1989), 3403-3410.* https://doi.org/10.1007/BF01139072
5) D. Wang, C. Yu, J. Ma, W. Liu, Z. Shen, Densification and crack suppression in selective laser melting of pure molybdenum, *Materials & Design, 129 (2017),* 44-52. http://doi.org/10.1016/j.matdes.2017.04.094
6) L. Kaserer, J. Braun, J. Stajkovic, K.H. Leitz, B. Tabernig, P. Singer, I. Letofsky-Papst, H. Kestler, G. Leichtfried, Fully dense and crack free molybdenum manufactured by Selective Laser Melting through alloying with carbon, *International Journal of Refractory Metals and Hard Materials, 84 (2019),* 105000. https://doi.org/10.1016/j.ijrmhm.2019.105000
7) D. Faidel, D. Jonas, G. Natour, W. Behr, Investigation of the selective laser melting process with molybdenum powder, *Additive Manufacturing, 8 (2015),* 88-94. https://doi.org/10.1016/j.addma.2015.09.002
8) J. Braun, L. Kaserer, J. Stajkovic, K.H. Leitz, B. Tabernig, P. Singer, P. Leibenguth, C. Gapan, H. Kestler, G. Leichtfried, Molybdenum and tungsten manufactured by selective laser melting: Analysis of defect structure and solidification

mechanisms, *International Journal of Refractory Metals and Hard Materials*, *84 (2019)*, 104999. https://doi.org/10.1016/j.ijrmhm.2019.104999

9) M. Higashi, T. Ozaki, Selective laser melting of pure molybdenum: Evolution of defect and crystallographic texture with process parameters, *Materials & Design*, *191* (2020), 108588. https://doi.org/10.1016/j.matdes.2020.108588
10) J.L. Johnson, T. Palmer, Directed energy deposition of molybdenum, *International Journal of Refractory Metals and Hard Materials*, *84* (2019), 105029. https://doi.org/10.1016/j.ijrmhm.2019.105029
11) A.J. Moorhead, J.R. DiStefano, R.E. McDonald, Fabrication procedures for unalloyed molybdenum, *Nuclear Technology*, *24*(1) (1974), 50-63. https://doi.org/10.13182/NT74-A31460
12) B. Tabernig, N. Reheis, Joining of molybdenum and its application, *International Journal of Refractory Metals and Hard Materials*, *28*(6) (2010), 728-733. https://doi.org/10.1016/j.ijrmhm.2010.06.008
13) J. Wang, J. Wang, Y. Li, D. Zheng, Progress of research on welding for molybdenum alloys, *High Temperature Materials and Processes*, *33*(3) (2014), 193-200. https://doi.org/10.1515/htmp-2013-0037
14) W.J. Sames, Additive Manufacturing of Inconel 718 using Electron Beam Melting: Processing, Post-Processing, & Mechanical Properties, *PhD Dissertation, Texas A&M University, 2015.*
15) B. Gustavsson, Effect of Beam Scan Length on Microstructure Characteristics of EBM Manufactured Alloy 718, *(2018).*
16) S.S, Al-Bermani, An investigation into microstructure and microstructural control of additive layer manufactured Ti-6Al-4V by electron beam melting, PhD *Dissertation, University of Sheffield, 2011.*
17) W.J. Sames, F. Medina, W.H. Peter, S.S. Babu, R.R. Dehoff, (2014). Effect of process control and powder quality on Inconel 718 produced using electron beam melting. In *8th Int. Symp. Superalloy 718 Deriv* (pp. 409-423). https://doi.org/10.1002/9781119016854.ch32
18) P. Frigola, O. Harrysson, T.J. Horn, H. West, R. Aman, J.M. Rigsbee, D.A. Ramirez, L. Murr, F. Medina, R.B Wicker, E. Rodriguez, Fabricating copper components. *Advanced Materials & Processes*, 127(7) (2014), 20-24.
19) C.L. Frederick, Control of Grain Structure in Selective-Electron Beam Melting of Nickel Based Superalloys, *PhD Dissertation, University of Tennessee, 2018.*
20) S. Tammas-Williams, P.J. Withers, I. Todd, P.B. Prangnell, The effectiveness of hot isostatic pressing for closing porosity in titanium parts manufactured by selective electron beam melting, *Metallurgical and Materials Transactions A*, 47 (2016), 1939-1946. https://doi.org/10.1007/s11661-016-3429-3
21) Bauereiß, T. Scharowsky, C. Körner, Defect generation and propagation mechanism during additive manufacturing by selective beam melting. *Journal of Materials Processing Technology*, *214*(11) (2014), 2522-2528. https://doi.org/10.1016/j.jmatprotec.2014.05.002
22) Z.C. Cordero, R.B. Dinwiddie, D. Immel, R.R. Dehoff, Nucleation and growth of chimney pores during electron-beam additive manufacturing. *Journal of Materials Science*, *52*(6) (2017), 3429-3435. https://doi.org/10.1007/s10853-016-0631-z
23) GE Additive Academy, L1 Training Operation and Maintenance Manual